JOURNAL OF APPLIED ELECTROCHEMISTRY 13 (1983) 623–635

Corrosion and polarization characteristics of zinc in battery electrolyte analogues and the effect of amalgamation

L. M. BAUGH, F. L. TYE, N. C. WHITE

Berec Group Limited, Group Technical Centre, St. Ann's Road, London N15 3TJ, UK

Received 20 October 1982

The corrosion and polarization characteristics of zinc have been investigated in concentrated NH_4Cl and NaCl solutions which represent suitable electrolyte analogues for Leclanché and zinc chloride cells, respectively. The effects of zinc amalgamation in the range 0–1 mg Hg cm^{-2} have also been examined and the results compared and contrasted with those obtained in concentrated KOH solution which is a useful electrolyte analogue for alkaline cells. It is shown that the structure of the zinc–solution interphase and the electrochemical reactions which occur are critically dependent upon the particular electrolyte considered. Despite this, the absolute corrosion rates of unamalgamated zinc are of the same order. This is an unexpected result. The effectiveness with which both dissolved zinc salts and mercury reduce the corrosion rate decreases in the electrolyte order

$$KOH \gtrsim NH_4Cl > NaCl$$

This is explained by the increasing participation of diffusion as the factor which controls the rate of the cathodic hydrogen evolution process. Maximum effectiveness for corrosion inhibition is approached when the mercury level exceeds 100 $\mu g\ cm^{-2}$. At this concentration, coverage of the surface by a zinc rich amalgam of almost constant composition is complete.

1. Introduction

Zinc is used extensively as an anode material in primary battery systems. Corrosion, however, occurs in all electrolytes and the partial remedy which is universally adopted is amalgamation of the zinc. Whilst the corrosion behaviour of unamalgamated zinc is relatively well understood both in neutral [1–3] and alkaline [4, 5] media, that of amalgamated zinc has been little investigated.

In a previous study [6] the corrosion and polarization characteristics of zinc were examined in concentrated KOH solution which represents a convenient electrolyte analogue for alkaline cell systems. It was shown that the detailed polarization characteristics can only be explained if due consideration is given to morphological changes on the zinc surface. It was concluded that a surface amalgam phase of almost constant composition is formed as the level of mercury increases and this determines the maximum corrosion efficiency which approaches 90% at the 1 mg Hg cm^{-2} level.

In the present paper we report an investigation in concentrated NH_4Cl and NaCl solutions which are suitable electrolyte analogues for the weakly acid Leclanché and zinc chloride cell systems, respectively. In order to eliminate interference from zinc deposition, which would otherwise dominate during cathodic polarization and obliterate hydrogen evolution characteristics, the analogue electrolytes have not contained dissolved zinc species. (Dissolved zinc salts are, of course, present in the complete battery electrolyte formulations). Where pertinent, the results are compared and contrasted with those obtained for the alkaline analogue.

2. Experimental procedure

2.1. *Electrode preparation and technique of amalgamation*

Electrode preparation prior to amalgamation was as described previously [1] except that the elec-

0021–891X/83 $03.00 + .12.

trodes were not chemically etched. Amalgamation was performed by electrodepositing mercury galvanostatically onto pure zinc electrodes (99.9999%) from KOH (1 mol dm^{-3}) saturated with yellow HgO at a current density of 10 mA cm^{-2}. During amalgamation the electrodes were either held stationary or rotated at 1000 rpm. The relationship between mercury deposited and time was determined analytically by flameless atomic absorption spectrophotometry after dissolving the amalgamated electrodes in conc. HNO_3. Linear relationships were established having slopes of 1.2 μg Hg cm^{-2} min^{-1} and 9.7 μg Hg cm^{-2} min^{-1} for stationary and rotating electrodes, respectively. In order to achieve greater accuracy during deposition of small quantities of mercury (< 10 μg cm^{-2}) stationary electrodes were employed.

2.2. *Cell and electrode assemblies*

The electrochemical cell, electrode assemblies and instrumentation have been described previously [1]. For impedance measurements, the counter electrode was a bright platinum disc situated directly below and parallel to the working electrode. The cell and electrode assemblies were situated inside a thermostatically controlled enclosure at 30 ± 0.1° C.

The reference electrode was $Hg | Hg_2Cl_2 | KCl$ (sat).

2.3. *Solutions*

NH_4Cl and NaCl solutions were prepared from twice recrystallized Analar grade salts using three times distilled water. Variations in pH were effected by the addition of small quantities of HCl, NH_4OH or NaOH to the working solutions. The ionic strength and pH of the solutions were adjusted so as to make them equivalent to those operating in the respective battery electrolytes. The composition of the solutions were as follows:

1. NH_4Cl (6.0 mol dm^{-3}, pH 5.3) the analogue for Leclanché cells.
2. NaCl (2.7 mol dm^{-3}, pH 4.8) the analogue for zinc chloride cells.

2.4. *Procedure*

Immediately after amalgamation the electrode was washed in distilled water and transferred to the electrochemical cell which contained the particular electrolyte analogue to be investigated. Short (high frequency) impedance spectra (values of $Z' = R_s$ and $Z'' = 1/\omega C_s$) were first recorded in the frequency range 20 KHz down to 1 KHz. From Z'' values at the highest frequencies almost constant (frequency independent) values of C_s were computed. These were then averaged to yield a mean value for the double layer capacity, C_{dl}. For each mercury level C_{dl} values were determined firstly as a function of time at constant potential and secondly, as a function of potential after an equilibration period.

Current–potential data were recorded by monitoring the current at fixed potential increments during slow potential sweeps (5 mV min^{-1}). The general procedure has been discussed previously [1]. Corrosion currents were obtained by Tafel line extrapolation, i_{corr}^{Ext}, and from the relationships derived by Stern and Geary [7]

$$i_{corr}^{R_p} = (1/2.3R_p)\{b_a b_c/(b_a + b_c)\} \quad (1)$$

where R_p is the polarization resistance, i.e., the slope of the current–potential line in the vicinity of the corrosion potential

$$R_p = (dE/di)_{i \to 0} \quad (2)$$

and b_a and b_c are the Tafel slopes for the anodic (zinc dissolution) and cathodic (hydrogen evolution) lines. A third corrosion current, i_{corr}^{Batt}, was obtained by extrapolating the cathodic Tafel line back to the open-circuit potential of zinc in the complete battery electrolyte formulation, i.e., containing the relevant zinc salt (saturated). Figure 1 shows schematically the relationships between i_{corr}^{Ext}, $i_{corr}^{R_p}$ and i_{corr}^{Batt}.

All experiments were duplicated and good reproducability was obtained. Quoted corrosion currents represent the mean of at least two independent determinations. Experiments were conducted under deaerated conditions.

3. Results and discussion

3.1. *Electron optical study*

Figure 2a illustrates the polycrystalline nature of a typical electrode surface which is revealed by chemical etching. It can be seen that the grain size is very large as would be expected for cast pure

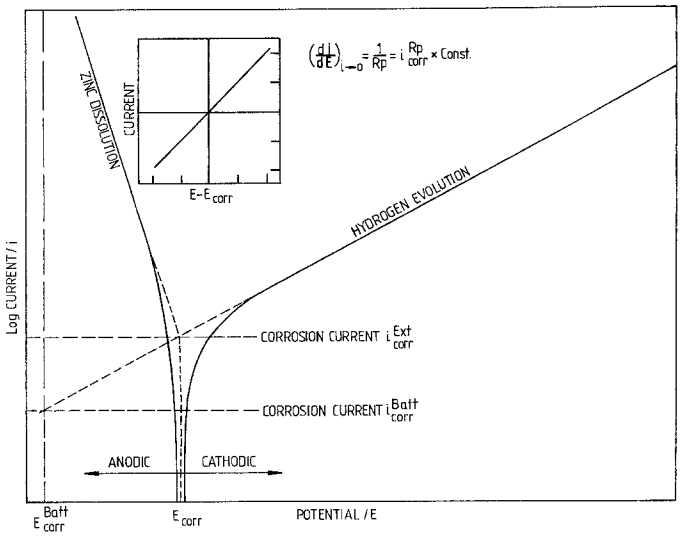

Fig. 1. Schematic representation of polarization curves and evaluation of corrosion parameters. E_{corr}, open-circuit/corrosion potential of zinc in analogue electrolyte. E_{corr}^{Batt}, open-circuit/corrosion potential of zinc in battery electrolyte.

zinc. Fig. 2b is an electron micrograph showing the polished metal surface prior to amalgamation and Figs. 2c–f are electron micrographs taken 3 h after amalgamation at different levels in the range 10 μg cm^{-2} to 1 mg cm^{-2}. At low mercury levels, the mercury deposits are localized with preferential deposition onto certain grains (Fig. 2c). Electron probe microanalysis confirmed the localized nature of the deposits and proved that the mercury concentration on the rest of the surface was below the detection limit. As the mercury level increases from 50–100 μg cm^{-2} there is an increase in the coverage of the deposit culminating in complete coverage at the 1 mg cm^{-2} level. These results suggest that deposition occurs by a mechanism involving the progressive nucleation and growth of three dimensional centres which overlap at long times.

Swift *et al.* [8] demonstrated that initial mercury penetration into Leclanché battery zinc alloy occurs by a grain boundary mechanism. A model was derived relating the surface concentration of mercury with time. This predicted a sharp fall in the concentration at short times followed by a slower fall at longer times. It must be emphasized, however, that in the present case, any reduction in the surface concentration will be much slower owing to the greatly diminished length/area of exposed grain boundaries, (Fig. 2a). Mercury penetration into the grains (or sub-grains) is thus considered to be the dominant factor controlling the change in surface concentration with time and the rate of this process is about seven orders of magnitude slower than grain boundary diffusion [8]. The surface concentration should, as a result, remain reasonably constant for long periods thereby facilitating electrochemical study.

3.2. *Double layer capacity and polarization characteristics*

3.2.1. NH_4Cl electrolyte analogue. Figure 3a shows the double layer capacity as a function of time for different amalgamation levels. Two trends are discernible from these results. Firstly, the capacity falls with time, the equilibration period being short and constant (*c.* 40 min). Secondly, the capacity decreases with increase in mercury concentration. Figure 3b shows the capacity as a function of cathodic potential. The shallow minimum present at all mercury levels confirms the absence of specific anion adsorption. However, the fall in capacity with mercury concentration is indicative of the presence of a second phase on the zinc surface which dominates the absolute magnitude of the capacity. Earlier work carried out on unamalgamated zinc in weakly acid solutions indicated that the metal is covered with an oxide/hydroxide layer at potentials close to the corrosion potential [9]. This results in the attainment of very low capacity values. Evidence was provided that in the presence of NH_4^+ ions the formation of such a film is inhibited. It was postulated that this results

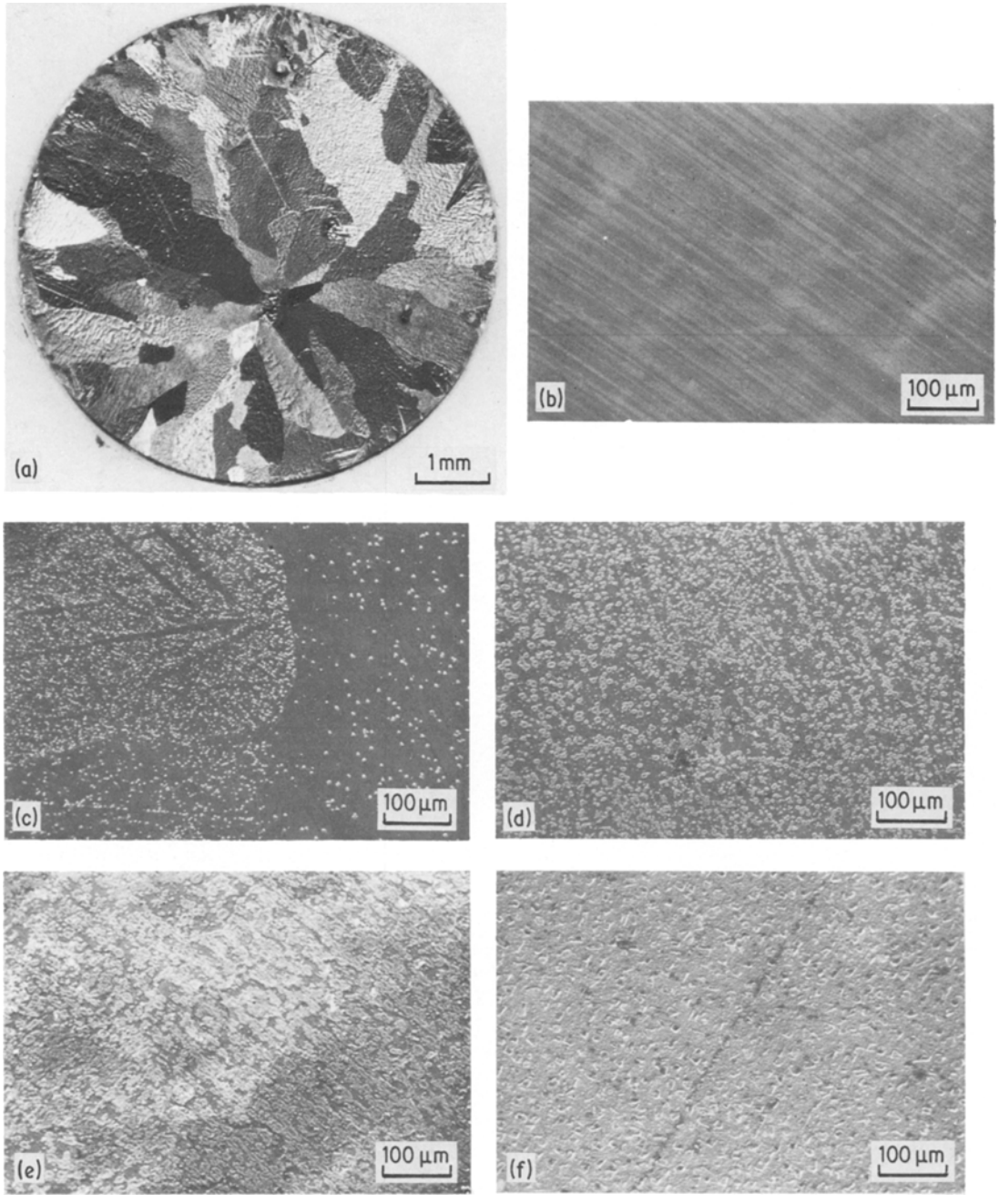

Fig. 2. Optical and scanning electron micrographs of zinc surface, (a) optical micrograph showing entire electrode area and grain structure after etching, (b) SEM showing polished surface prior to amalgamation, (c)–(f) SEMS showing surface after amalgamation to (c) 10 μg cm^{-2}, (d) 50 μg cm^{-2}, (e) 100 μg cm^{-2}, (f) 1000 μg cm^{-2}.

from the dissociation of NH_4^+ ions in the double layer which effectively decreases the pH at the metal surface below the critical value for film formation. Figure 3c is in complete agreement with these conclusions where it can be seen that the capacity is close to 40 μF cm^{-2} for unamalgamated zinc, a value typical of that for a film-free surface [6]. The decrease in capacity infers that either the thickness of the film or coverage of the metal by the film increases with mercury

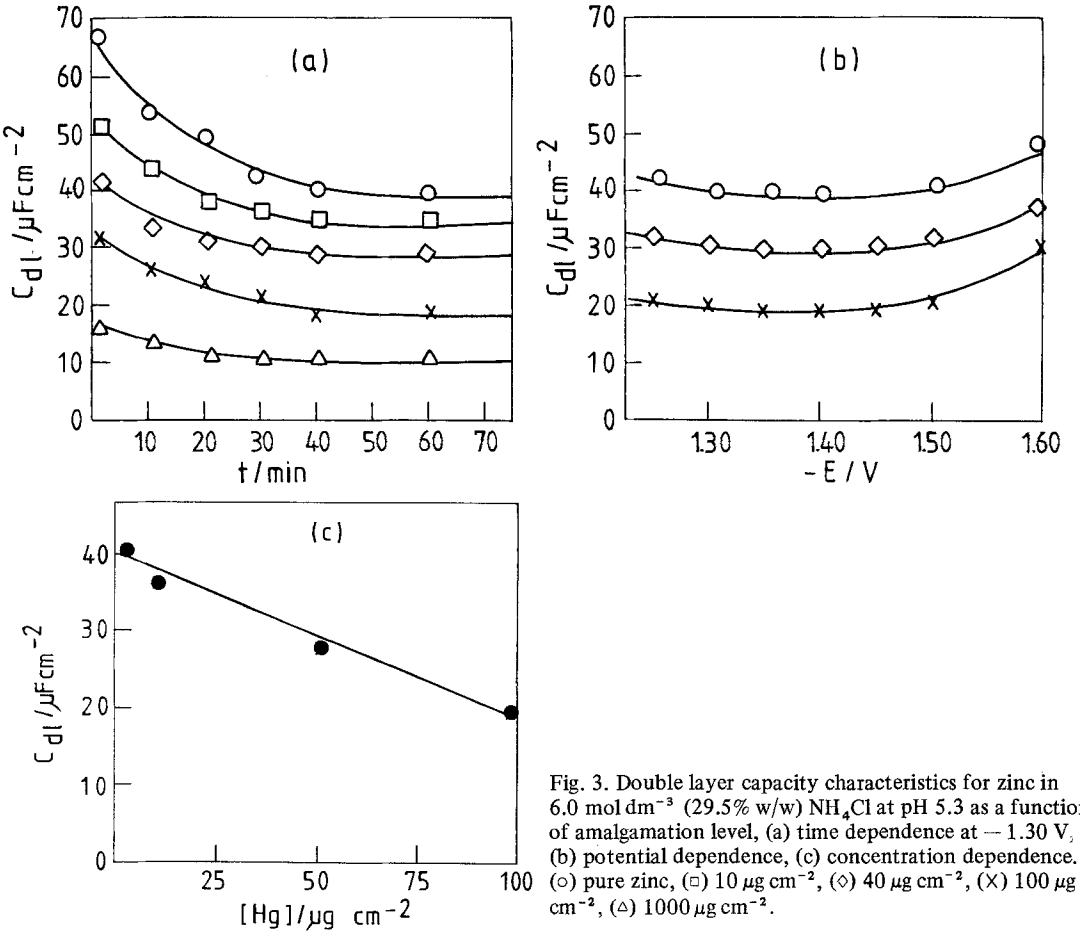

Fig. 3. Double layer capacity characteristics for zinc in 6.0 mol dm^{-3} (29.5% w/w) NH_4Cl at pH 5.3 as a function of amalgamation level, (a) time dependence at −1.30 V, (b) potential dependence, (c) concentration dependence. (○) pure zinc, (□) 10 μg cm^{-2}, (◇) 40 μg cm^{-2}, (×) 100 μg cm^{-2}, (△) 1000 μg cm^{-2}.

concentration and that a limiting situation is approached at concentrations > 1 mg cm^{-2} (Fig. 3a). Since it is known that coverage of the zinc surface by a zinc amalgam phase also increases with mercury concentration (Fig. 2) then coverage is the important factor. It can, therefore, be concluded that the capacity characteristics of Fig. 2 result from the replacement of an oxide-free zinc surface with an oxidized amalgamated surface. If $C_{Zn/Hg}$ is the double layer capacity per unit area associated with the surface amalgam phase and C_{Zn} that associated with the uncovered zinc surface, then the measured capacity can be approximated by the expression used previously [6]

$$C_{dl} = C_{Zn}(1-\theta) + C_{Zn/Hg}\,\theta \qquad (3)$$

where θ is the fractional surface coverage. Here, $C_{Zn/Hg} < C_{Zn}$ and hence C_{dl} decreases with θ.

The dependence of C_{dl} upon amalgamation level in NH_4Cl solutions is opposite to what is observed in KOH solutions since the capacity *rises* to a plateau at the 1 mg cm^{-2} level in the latter [6]. In the case of alkaline solutions, oxides are not formed even at the highest amalgamation levels and therefore the rise in capacity has been attributed to an increase in area of the amalgamated parts of the zinc surface, i.e., $C_{Zn/Hg} > C_{Zn}$ [6]. It may be concluded from these comparisons that when the amalgam phase is oxide coated, the absolute magnitude of $C_{Zn/Hg}$ is determined primarily by the thickness of the oxide layer and changes in amalgam/oxide interfacial area are of secondary importance.

Figure 4 shows the anodic and cathodic polarization characteristics for zinc dissolution and hydrogen evolution, respectively, as a function of mercury level. It is clear that the anodic behaviour is complex since both the position and slope of the curves are affected. This is in contrast with the behaviour in KOH solution [6] where the anodic characteristics show little depen-

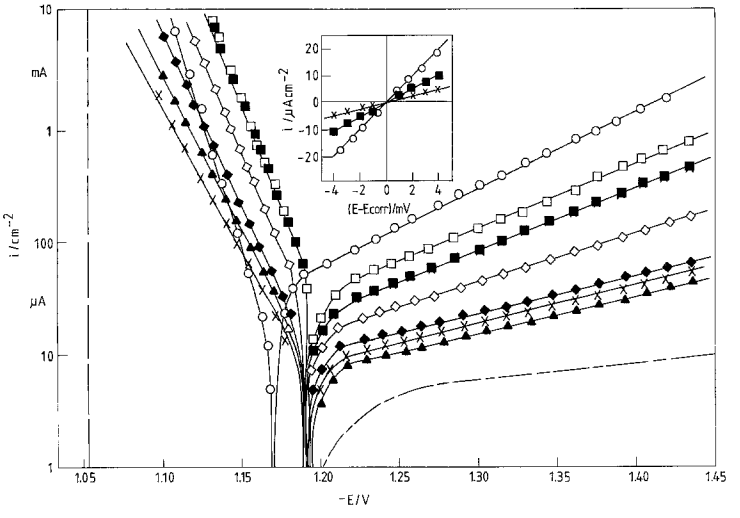

Fig. 4. Polarization characteristics for zinc in 6.0 mol dm^{-3} (29.5% w/w) NH_4Cl at pH 5.3 as a function of amalgamation level, (○) pure zinc, (□) 10 $\mu g\ cm^{-2}$, (■) 20 $\mu g\ cm^{-2}$, (◇) 40 $\mu g\ cm^{-2}$, (◆) 75 $\mu g\ cm^{-2}$, (×) 100 $\mu g\ cm^{-2}$, (▲) 1000 $\mu g\ cm^{-2}$. (———) Cathodic curve for 6% (w/w) Zn in Hg amalgam.

dence upon amalgamation level above 10 $\mu g\ cm^{-2}$. Also, the extent to which the cathodic hydrogen evolution current is diminished by mercury in the NH_4Cl solution is somewhat smaller than in the alkaline electrolyte and the slopes of the cathodic lines are increased more severely. Figure 5 demonstrates that diffusion plays a role in determining the polarization characteristics but in a complex manner since the diffusion effects are dependent upon whether the metal is amalgamated or unamalgamated. Hence, the curves of Fig. 4 are influenced by amalgamation level in a complex manner which depends upon both the film forming ability of the metal surface and diffusion effects in solution. The overall reactions which control the corrosion rate of zinc in the electrolyte analogue of the Leclanché cell can be represented

$$Zn + 4Cl^- \rightleftharpoons ZnCl_4^{2-} + 2e \qquad (4)$$

$$2NH_4^+ + 2e \rightarrow 2NH_3 + H_2 \qquad (5)$$

$$Zn + 2NH_4^+ + 4Cl \rightarrow ZnCl_4^{2-} + 2NH_3 + H_2 \qquad (6)$$

Here the product $ZnCl_4^{2-}$ is written as the most likely complex but others could be involved. The anodic and cathodic branches of the polarization curves will now be discussed separately in more detail.

It is clear from Fig. 4 that except for levels $< 20\ \mu g\ cm^{-2}$ the dischargeability of zinc in NH_4Cl solution decreases with mercury concentration. This is an unexpected result and suggests that the factor responsible is the oxide/hydroxide film present on the amalgamated parts of the electrode surface. This conclusion is reinforced by Fig. 6 which shows that there is a clear relationship between anodic current and double layer capacity at a constant potential (— 1.12 V) and

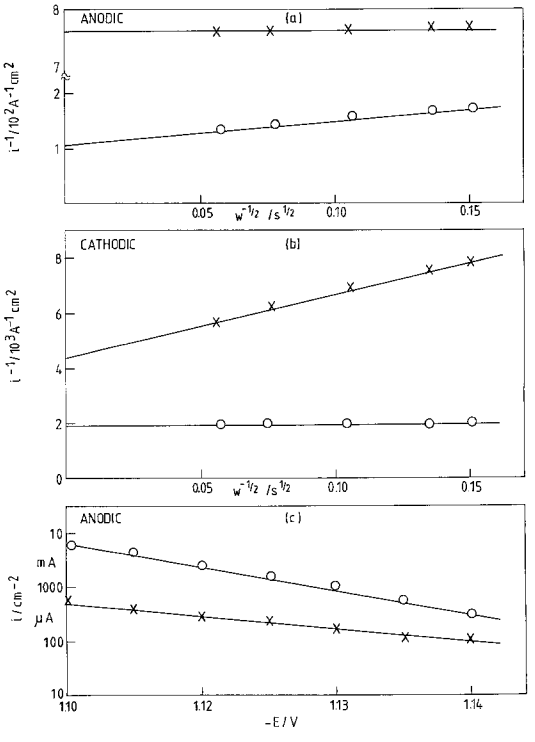

Fig. 5. Rotation speed (w) dependence of anodic and cathodic currents on (○) pure zinc and (×) amalgamated (100 $\mu g\ cm^{-2}$) zinc in 6.0 mol dm^{-3} (29.5% w/w) NH_4Cl at pH 5.3, (a) anodic currents at — 1.11 V, (b) cathodic current at — 1.30 V, (c) anodic Tafel lines extrapolated to infinite rotation speed.

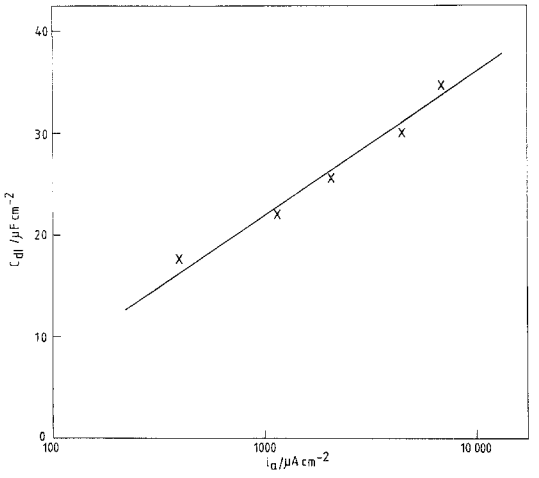

Fig. 6. Plot of double layer capacity v. anodic current at − 1.12 V for zinc dissolution in 6.0 mol dm^{-3} (29.5% w/w) NH_4Cl at pH 5.3. Symbols as in Fig. 4.

therefore the same factor is responsible for variations in both parameters. Figure 4 also shows that the slopes of the anodic lines change from 30 mV per decade ($2.3 \times RT/2F$) at amalgamation levels 0–20 μg cm^{-2} which are indicative of a reversible exchange process, to 40 mV per decade ($2.3 \times 2RT/3F$) indicative of an irreversible dissolution process [2]. These conclusions are confirmed from the rotation speed dependence of the anodic current shown in Fig. 5a which demonstrates that the current is independent of rotation speed for heavily amalgamated zinc. These results indicate that on the amalgamated surface the oxide/hydroxide film either inhibits the general rate of dissolution to the extent that the process becomes charge transfer controlled or that the dissolution process becomes inherently irreversible as a result of a severe diminution in the rate of zinc deposition. Nevertheless, it is clear from Fig. 4 that the electrode is not *passivated*. Further, there is no suggestion that the rate of dissolution ever becomes limited by film resistance effects. It may, therefore, be more useful to consider that in the case of pure zinc in the NH_4Cl solution the electrode is covered with a densely packed layer of adsorbed intermediates of the form $ZnOH_{ads}$ the existence of which can be inferred from impedance measurements [10]. Such a layer might be expected to exhibit a transition in its properties from those of an adsorbed intermediate at low coverages to those of a surface compound at high coverages. It is postulated that a change of this kind could be induced more easily on amalgamated zinc where the density of active sites would be higher thus facilitating the formation of a surface compound.

Hydrogen evolution on metals of high hydrogen-overvoltage in near neutral solutions of ammonium salts occurs via the reduction of NH_4^+ ions [2, 11]. Although the overall reaction may be represented by Equation 5 the precise mechanism is as yet not fully understood. That protons can be derived from NH_4^+ ions present at the outer Helmholtz plane has been discussed previously. Also, in near neutral $NH_4Cl/NaCl$ solutions of constant ionic strength, the hydrogen-overvoltage does not decrease in any monotonic sense with NH_4^+ ion concentration [12] suggesting that dissociation could play a part in the mechanism of hydrogen evolution

$$NH_4^+ + H_2O \rightleftharpoons NH_3 + H_3O^+ \qquad (7)$$

Nevertheless, the rate determining step (rds) is likely to be

$$NH_4^+ + e \rightarrow NH_3 + H_{ads} \qquad \text{(rds)} \qquad (8)$$

followed by

$$H_{ads} + H_3O^+ + e \rightarrow H_2 + H_2O \qquad (9)$$

That reaction 8 proceeds under charge transfer controlled conditions for pure zinc is confirmed by the observation of a Tafel slope close to $2.3 \times 2RT/F$ in Fig. 4. It may be supposed that inhibition of the overall Reaction 5 occurs via a reduction in the $Zn–H_{ads}$ bond energy for Reaction 8 as discussed by Bockris and Reddy [13] for the case of acid solutions. Figure 4 shows that as the mercury concentration increases the Tafel slope also increases as in the case of the alkaline analogue [6]. However, the factors which contribute to this observation are more numerous. Figure 5 demonstrates that when the concentration of mercury becomes appreciable the cathodic current becomes rotation speed dependent. This infers that the rate of Reaction 8 is sufficiently inhibited that it approaches the rate of the parallel bulk proton reduction process which is diffusion limited. Using a 6% (w/w) Zn in Hg liquid amalgam in the form of a hanging drop electrode, it is possible to eliminate charge transfer controlled NH_4^+ ion reduction and reveal the diffusion limited

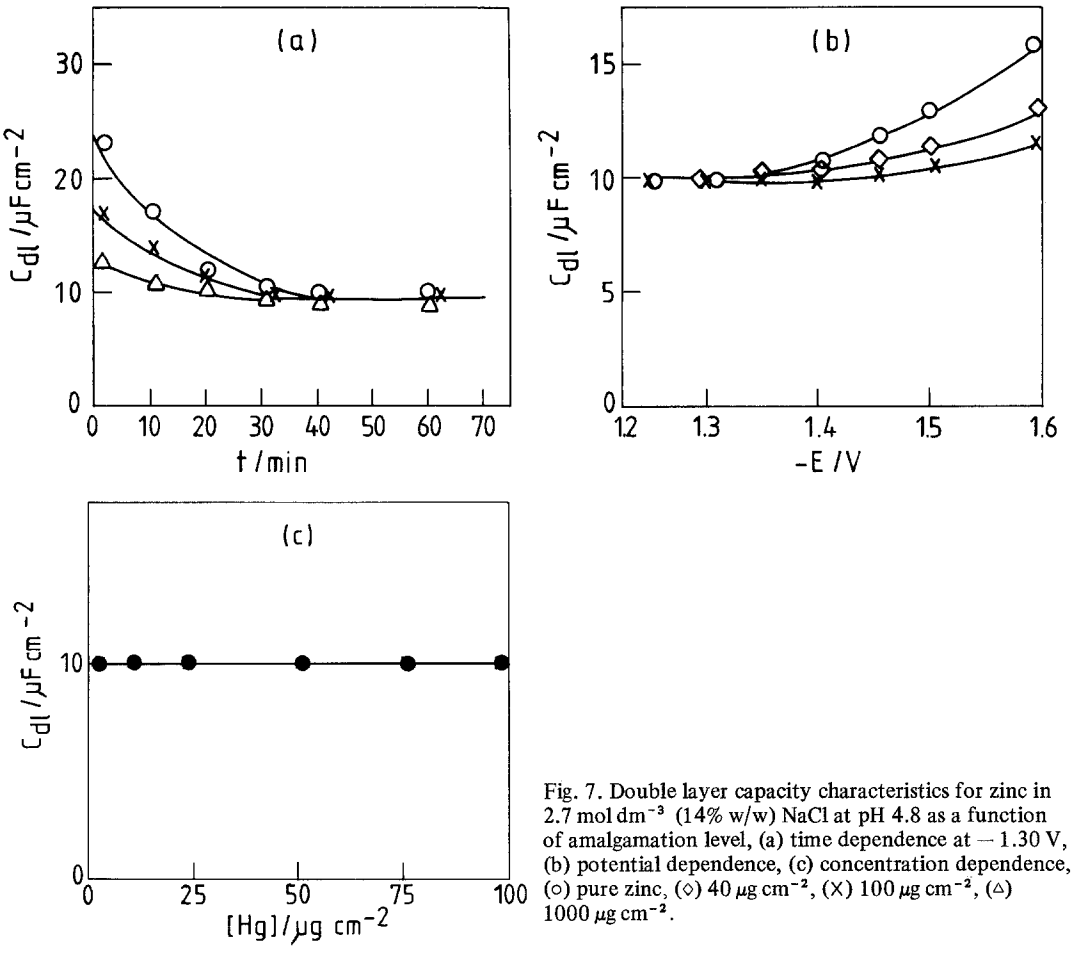

Fig. 7. Double layer capacity characteristics for zinc in 2.7 mol dm^{-3} (14% w/w) NaCl at pH 4.8 as a function of amalgamation level, (a) time dependence at − 1.30 V, (b) potential dependence, (c) concentration dependence, (○) pure zinc, (◇) 40 μg cm^{-2}, (×) 100 μg cm^{-2}, (△) 1000 μg cm^{-2}.

H_3O^+ reduction current alone. This is also shown in Fig. 4. Extrapolation of the cathodic curves to infinite rotation speed produces Tafel slopes of a similar order to those for the KOH analogue, namely 220 mV per decade [6]. Whilst surface heterogeneity effects [14] may be expected to play a role in both the NH_4Cl and KOH solutions, the high slopes observed in the former electrolyte may also be due in part to the presence of the oxide film if this is not cathodically reduced [15].

A comparison of the cathodic polarization characteristics displayed in Fig. 4 for NH_4Cl with those obtained previously for KOH solutions [6] reveals the unexpected result that they are qualitatively very similar. Also, the rate of hydrogen evolution cannot be lowered by more than an order of magnitude in either electrolyte. These observations are surprising in view of the fact that the electroactive species involved and reaction mechanisms are reported to be quite different. This problem may be resolved if it is assumed that the common factor controlling the overvoltage is the Zn–H_{ads} bond energy [13]. However, if this conclusion is correct, then it casts some doubts upon the validity of the *chemical* mechanism of hydrogen evolution proposed by several authors for alkaline solution [4, 5] since the Zn–H_{ads} bond energy would not be expected to affect the rate determining step in this mechanism. The hydrogen overvoltage data reported in the present and previous communications therefore supports the view that in alkaline media, at potentials close to the open circuit value, H_2O molecules react electrochemically to produce adsorbed hydrogen in the rate determining step, (see Equation 13).

3.2.2. NaCl electrolyte analogue. Figure 7a shows the double layer capacity of zinc at a constant cathodic potential as a function of time

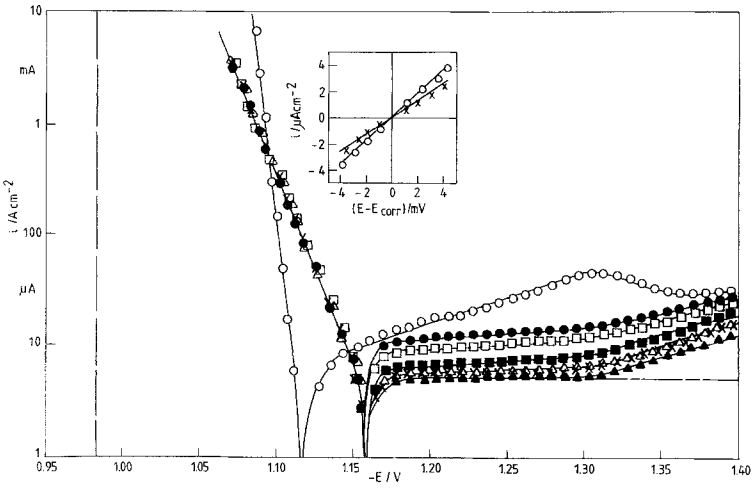

Fig. 8. Polarization characteristics for zinc in 2.7 mol dm^{-3} (14% w/w) NaCl at pH 4.8 as a function of amalgamation level, (○) pure zinc, (●) 5 $\mu g\ cm^{-2}$, (□) 10 $\mu g\ cm^{-2}$, (■) 20 $\mu g\ cm^{-2}$, (△) 50 $\mu g\ cm^{-2}$, (X) 100 $\mu g\ cm^{-2}$, (▲) 1000 $\mu g\ cm^{-2}$. (– – –) Cathodic curve for 6% (w/w) Zn in Hg amalgam.

for different amalgamation levels. The results are quite different to those in both KOH and NH_4Cl analogues but show greater similarities with the latter (cf. Fig. 3a). Thus, the capacity falls with time. However, unlike the NH_4Cl electrolyte the capacity is independent of mercury concentration being in all cases very low and close to 10 $\mu F\ cm^{-2}$. Figure 7b also demonstrates that the capacity shows little, if any, dependence upon potential. These characteristics are consistent with the view that in the NaCl analogue an oxide/hydroxide film of uniform coverage is present on the zinc independent of amalgamation level. Relation 3 applies with $C_{Zn/Hg} = C_{Zn}$, i.e., C_{dl} is independent of θ. The insensitivity of the Zn/NaCl system to mercury concentration contrasts strongly with that of the Zn/NH_4Cl system and indicates that the film inhibiting properties engendered by NH_4^+ ion dissociation contributes to the differences observed.

Figure 8 shows the anodic and cathodic polarization characteristics for zinc dissolution and hydrogen evolution, respectively, as a function of the mercury level. In contrast with the curves for NH_4Cl solutions, it is clear that the anodic branches of the curves are independent of amalgamation level for concentrations $> 5\ \mu g\ cm^{-2}$ and the cathodic branches are only slightly affected. Except for the case of pure zinc the anodic slopes are close to $2.3 \times RT/2F$ indicative of a reversible dissolution process whilst the cathodic slopes approach ∞ demonstrating that hydrogen evolution occurs via diffusion limited proton reduction from bulk solution. The overall reactions which dictate the corrosion rate of zinc in the electrolyte analogue of the zin chloride cell can be represented

$$Zn + 4Cl^- \rightleftharpoons ZnCl_4^{2-} + 2e \qquad (10)$$

$$2H_3O^+ + 2e \rightarrow H_2 + 2H_2O \qquad (11)$$

$$Zn + 4Cl^- + 2H_3O^+ \rightarrow ZnCl_4^{2-} + 2H_2O + H_2 \qquad (12)$$

Here, the product $ZnCl_4^{2-}$ is written by analogy with $Zn(OH)_4^{2-}$ formed in alkaline media although other anion complexes could be involved. As in the case of the NH_4Cl solution, the anodic and cathodic branches of the curves will be discussed separately.

The characteristics of zinc dissolution displayed in Fig. 8 present considerable difficulties of interpretation in view of their dissimilarity with those of either the Zn/KOH or Zn/NH_4Cl systems. The slopes of the anodic branches of the curves change from 12 mV per decade to a constant value of 30 mV per decade as the mercury concentration increases from 0–5 $\mu g\ cm^{-2}$. Over the same concentration range, the absolute magnitude of the current increases substantially, particularly at potentials close to the corrosion potential. Previous work [1] showed that the anodic slopes observed for pure zinc in weakly acid solutions (pH 5–6) reflect an *activation* of the oxide covered electrode as the anodic potential increases and this phenomenon appears to be specific to Cl^- containing electrolytes. This could result from a progressive displacement of film species by strongly adsorbed Cl^- ions. In the case of the amalgamated

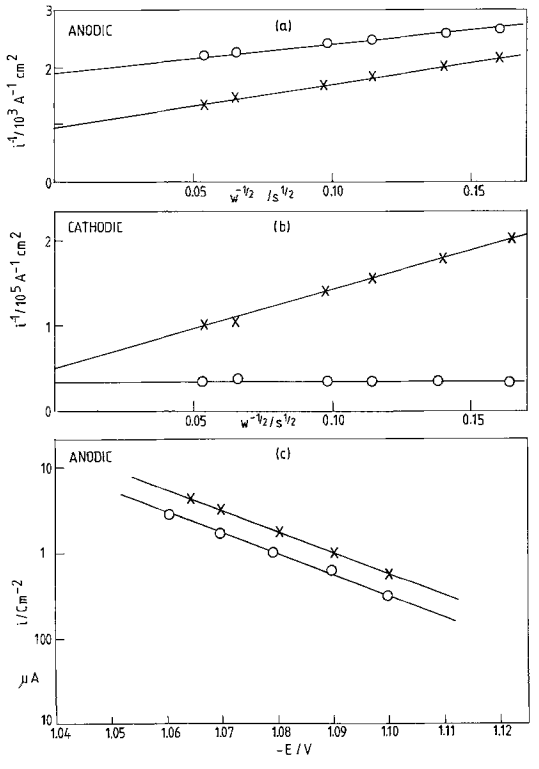

Fig. 9. Rotation speed (ω) dependence of anodic and cathodic currents on (o) pure zinc and (X) amalgamated (100 $\mu g\ cm^{-2}$) zinc in 2.7 mol dm^{-3} (14% w/w) NaCl at pH 4.8, (a) anodic current at − 1.09 V, (b) cathodic current at − 1.225 V, (c) anodic Tafel lines extrapolated to infinite rotation speed.

zinc, however, there is no evidence of such an activation. In fact, the general characteristics are typical of a film-free system being similar to those observed in the case of the KOH analogue. Further evidence of the validity of this conclusion is provided by the rotation speed dependence of the anodic current shown in Fig. 9a which indicates that although the current for both pure zinc and amalgamated zinc is strongly rotation dependent, Tafel lines having identical slopes of magnitude 40 mV per decade are produced by extrapolation to infinite speed (Fig. 9c). Since these lines are only slightly displaced from each other, the results infer that removal of the oxide/hydroxide film present on the pure zinc electrode is apparently facilitated by stirring. It is difficult to reconcile these conclusions with those reached from capacity measurements. However, it is possible that an activation of the amalgamated electrodes becomes feasible at potentials positive of where the capacity measurements were made, namely − 1.30 V. This would correspond to the point where the metal begins to dissolve and includes the open-circuit potential itself.

The cathodic hydrogen evolution characteristics displayed in Fig. 8 are considerably more complex than those for the other analogues. For pure zinc at potentials between − 1.15 and − 1.30 V, a Tafel line of high slope (260 mV per decade) appears. Since the current is not dependent upon electrode rotation speed (Fig. 9b) then this slope is consistent with the charge-transfer controlled reduction of water on an oxide coated electrode with reaction sequence given by Reactions 13 and 14.

$$H_2O + e \rightarrow H_{ads} + OH^- \text{ (rds)} \qquad (13)$$

$$H_{ads} + H_2O + e \rightarrow H_2 + OH^- \qquad (14)$$

At a potential of − 1.30 V, however, there is evidence for a partial removal of the film since a reduction peak is evident. As the level of amalgamation is increased to 5 $\mu g\ cm^{-2}$, there is a sharp change in the polarization profiles and at the highest level (1 mg cm^{-2}) a limiting current is clearly evident at low potentials. This changes to a Tafel line with slope 260 mV per decade at − 1.30 V. Thus, in the case of the heavily amalgamated electrode, hydrogen is evolved via diffusion limited proton reduction at low potentials (Reaction 11) and charge transfer controlled water reduction at high potentials. Hence, at low potentials, amalgamation reduces the rate of water reduction to such an extent that it becomes small compared with the rate of the parallel proton reduction process which, therefore, dominates the hydrogen evolution characteristics.

The change in the mechanism of hydrogen evolution at low potentials from water reduction for pure zinc to proton reduction for amalgamated zinc may explain why oxide/hydroxide film formation is facilitated on the former. Thus, it can be seen from a comparison of Reactions 14 and 11 together with a consideration of Fig. 8, that whereas OH^- ions are formed at the metal surface as a major product of hydrogen evolution on pure zinc, they will not be a major product on amalgamated zinc.

Table 1. Summary of corrosion rates

Mercury concentration	*Electrolyte*								
	KOH			*NH_4Cl*			*NaCl*		
(μg cm^{-2})	$i_{corr}^{R_p}$ (μA cm^{-2})	i_{corr}^{Ext} (μA cm^{-2})	i_{corr}^{Batt} (μA cm^{-2})	$i_{corr}^{R_p}$ (μA cm^{-2})	i_{corr}^{Ext} (μA cm^{-2})	i_{corr}^{Batt} (μA cm^{-2})	$i_{corr}^{R_p}$ (μA cm^{-2})	i_{corr}^{Ext} (μA cm^{-2})	i_{corr}^{Batt} (μA cm^{-2})
0	21.1	21.6	5.8	28.2	25.9	4.7	8.7	8.5	4.9
10	20.1	22.2	6.4	24.3	25.2	4.1	8.3	8.2	4.9
20	20.0	21.0	6.5	19.2	17.5	3.3	6.0	5.6	4.9
50	29.2	31.4	10.6	12.6	12.4	2.9	4.9	5.4	4.9
100	8.1	6.6	2.1	8.6	10.0	2.3	5.2	5.5	4.9
1000	2.3	2.1	0.85	8.9	9.9	2.2	4.9	5.6	4.9

4.3. *Comparison of corrosion rates and effectiveness of amalgamation*

Table 1 provides a summary of corrosion rates in deaerated solutions of the three electrolytes studied to date. Irrespective of which analogue is considered good, agreement between $i_{corr}^{R_p}$ and i_{corr}^{Ext} values. This indicates that the correct assumptions have been made regarding both the position and slopes of the relevant cathodic Tafel lines pertaining at the corrosion potential of zinc. Table 1 also shows that in the case of the KOH analogue the corrosion current is not reduced until the amalgamation level reaches $100\,\mu g\,cm^{-2}$. This has been attributed to an increase in the active area of the electrode at intermediate mercury concentrations which increases hydrogen evolution and opposes the process of corrosion inhibition [6]. It is by no means clear, however, why such an effect is not observed in the case of the other analogues since it can be assumed that for any given mercury level, the initial surface morphology of the zinc electrode was highly reproducible in all investigations. It is possible that in the case of the NH_4Cl analogue, compensation for increases in geometrical area is provided by oxide/hydrogen film formation which inhibits the anodic dissolution component of the corrosion process (Fig. 4) thereby, decreasing the corrosion current. In the case of the NaCl analogue, the corrosion rate is diffusion limited and it may be supposed that under these circumstances the corrosion current will not respond to changes in real electrode area or surface roughness.

Table 1 compares values for the corrosion rates i_{corr}^{Ext} and i_{corr}^{Batt} as a function of amalgamation level. For any given electrolyte analogue, the differences between these two values provided a measure of the effectiveness of the respective dissolved zinc salts, e.g., K_2ZnO_2 (alkaline cells) or $ZnCl_2$ (Leclanché and zinc chloride cells), for providing corrosion protection in a battery environment. Table 1 also indicates the effectiveness of mercury for reducing the corrosion rate as a function of mercury concentration.

4. Conclusion

From Table 1 and the preceeding discussion the following conclusions can be drawn:

1. The absolute corrosion rates in the various electrolyte analogues are of a similar order despite the fact that the cathodic processes which cause corrosion occur via different mechanisms. This is an unexpected result.

2. The presence of oxide/hydroxide layers on the zinc surface does not significantly affect the corrosion rate. This results from the semi-conducting nature of these films with respect to the cathodic process.

3. Dissolved zinc salts provide a measure of protection against corrosion in the case of the KOH and NH_4Cl electrolytes (60–80% reduction) by shifting the corrosion potential to more anodic values.

4. The effectiveness (efficiency) with which mercury reduces the corrosion rate decreases in the electrolyte order:

$$KOH \gtrsim NH_4Cl > NaCl$$

This is explained by the increasing participation of diffusion as the factor which controls the rate of the cathodic process.

5. In the case of the KOH and NH_4Cl electrolytes, the efficiency values depend little upon choice of i_{Batt}^{Ext} or i_{corr}^{Batt} in the calculation. This is due to the fact that the cathodic Tafel lines in these systems are almost parallel.

6. Maximum effectiveness for corrosion inhibition is approached when the mercury level exceeds $100\,\mu g\,cm^{-2}$. At this concentration, coverage of the zinc surface by a zinc rich amalgam of almost constant composition is complete.

Acknowledgements

The authors wish to thank the Directors of the Berec Group Limited for permission to publish this paper.

References

[1] L. M. Baugh, *Electrochim. Acta* **24** (1979) 657.
[2] *Idem, ibid.* **24** (1979) 669.
[3] K. G. Boto and L. F. G. Williams, *J. Electroanal. Chem.* 77 (1977) 1.
[4] L. Z. Vorkapic, D. M. Drazic and A. R. Despic, *J. Electrochem. Soc.* **121** (1974) 1385.
[5] V. S. Muralidharan and K. S. Rajagopalan, *J. Electroanal. Chem.* **94** (1978) 21.
[6] L. M. Baugh, F. L. Tye and N. C. White, Paper No. 21. 'Proceedings of the 13th International Power Sources Symposium', Brighton (1982).

To be published in 'Power Sources 9' (edited by J. Thomson), Academic Press, London (1983).
[7] M. Stern and A. L. Geary, *J. Electrochem. Soc.* **104** (1957) 56.
[8] J. Swift, F. L. Tye, A. M. Warwick and J. T. Williams, 'Power Sources 4' (edited by D. H. Collins), Oriel Press, Newcastle upon Tyne (1972) p. 415.
[9] L. M. Baugh and J. A. Lee, *J. Electroanal. Chem.* **48** (1973) 55.
[10] C. Cachet and R. Wiart, *ibid.* **129** (1981) 103.
[11] S. E. Ostrovskaya, E. G. Tsventarnyi and Ya. V. Durdin, *Elektrokhimiya* **9** (1973) 1275.
[12] L. M. Baugh and A. Higginson, unpublished work.
[13] J. O'M. Bockris and A. K. N. Reddy, 'Modern Electrochemistry', Vol. 2, Plenum Press, New York (1970) p. 1153.
[14] I. A. Ammar and S. Dawish, *Electrochim. Acta* **12** (1967) 833.
[15] A. K. Vijh, 'Electrochemistry of Metals and Semiconductors', Marcel Dekker Inc., New York (1973) p. 169.